Heliyon 10 (2024) e26213

Contents lists available at ScienceDirect

Heliyon

journal homepage: www.cell.com/heliyon

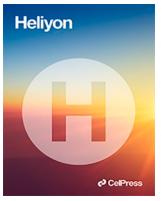

Research article

Biomechanical analysis of titanium-alloy and biodegradable implants in dual plate osteosynthesis for AO/ASIF type 33-C2 fractures

Mengmeng Hu [a,1], Meng Li [a,1], Rui Ma [b,1], Xiaoya Li [a], Xiaomeng Ren [c], Longbo Du [c], Chuyang Zeng [c], Jiantao Li [a,**], Wei Zhang [a,*]

[a] *Senior Department of Orthopedics, the Fourth Medical Center of PLA General Hospital, No. 51 Fucheng Road, Beijing, 100048, China*
[b] *Hainan Hospital of PLA General Hospital, No.80 Jianglin Road, Sanya, Hainan Province, 572013, China*
[c] *Medical School of PLA General Hospital, No. 28 Fuxing Road, Beijing, 100853, China*

A B S T R A C T

Background and objective: Treating geriatric osteoporotic distal femur fractures has always presented challenges, but developing biodegradable materials has brought new opportunities for therapeutic intervention. Despite this progress, there currently needs to be more evidence-based biomechanical guidelines for using dual plate fixation and biodegradable materials in treating osteoporotic comminuted distal femoral fractures. In this study, finite element analysis was conducted to evaluate the mechanical effectiveness of different implant materials (titanium alloys, biodegradable materials, and combinations of both) in the fixation of physiological and osteoporotic distal femoral fractures.

Methods: We constructed finite element models of 33-C2 fractures and three types of plates: the Lateral Less Invasive Stabilization System (LISS) plate, the titanium-alloy medial plate (TAP), and the biodegradable plate (BP). To evaluate the biomechanical advantages in both physiological femur (PF) and osteoporotic femur (OF) conditions, three scenarios were developed: LISS + TAP, LISS + BP, and double biodegradable plates (DBPs). Five loading conditions were applied to measure structural stiffness, fracture micromotion, and implant stress: medio-lateral four-point bending, antero-posterior four-point bending, axial loading, torsional loading, and sideways falling. Several parameters were examined, including peak Von Mises Stress (VMS) of the femur and lateral plate, maximum displacement, bending angle, torsional angle of fracture, and risk of fracture.

Results: In four-point bending tests, the lateral plate of the DBPs group exhibited a slightly lower peak VMS compared to the LISS + TAP and LISS + BP groups. When subjected to axial loading, the stiffness values of the LISS + TAP (OF) were 1.42 times and 1.86 times higher than LISS + BP (OF) and DBPs (OF) groups, and the peak VMS of lateral plate of DBPs (OF) construct was approximately 2% and 16% lower than that of the LISS + TAP (OF) and LISS + BP (OF) constructs. Under torsional loading, DBPs (OF) demonstrated rotational stiffness that was respectively 2% and 52% greater than that of LISS + TAP (OF) and LISS + BP (OF). Regarding the peak VMS of femur, the values of DBPs (OF) were almost 8% and 15% lower than those of LISS + TAP (OF) and LISS + BP (OF).

Conclusions: The use of DBPs at 11.33 GPa facilitated early mobilization of load-bearing joints but exhibited limited ability to support full weight-bearing activities. Though LISS + TAP met practical strength requirements, one should consider the potential biological irritation and stress shielding. Thus, employing a combination of biodegradable and metal internal fixation is a valid approach to effectively treat weight-bearing joint fractures in clinical practice.

* Corresponding author. The Fourth Medical Center of PLA General Hospital, No. 51 Fucheng Road, Beijing, 100048, China.
** Corresponding author. The Fourth Medical Center of PLA General Hospital, No. 51 Fucheng Road, Beijing, 100048, China.
E-mail addresses: lijiantao618@163.com (J. Li), bszw@hotmail.com (W. Zhang).
[1] The first three authors contributed equally to this work.

https://doi.org/10.1016/j.heliyon.2024.e26213
Received 6 June 2023; Received in revised form 4 January 2024; Accepted 8 February 2024
Available online 14 February 2024

1. Introduction

Distal femur fractures comprise around 3–6% of all fractures in the femur [1,2], ranking as the second most prevalent fractures in the femur, following proximal fractures [3]. These fractures are prevalent in young patients with high-energy trauma or geriatric individuals due to low-velocity injuries [4]. However, about 15–20% of distal femur fractures may result in complications, such as osteonecrosis, infection, and even mortality [5–7]. The rising incidence of these fractures places a growing social and economic burden on society [8]. Elderly patients, in particular, are prone to poor bone quality, which can attributed to systemic illnesses, osteoporosis, or stress shielding caused by prostheses, which can contribute to complications such as prosthetic loosening, prosthetic removal, nonunion, or malunion [9,10]. It is noted that the mortality rate in elderly patients who undergo distal femoral fracture surgery can reach 30% within the first year [3,11], which may be related to a lack of postoperative weight-bearing training.

Although locking plates are the preferred choice for internal fixation in fractures of the comminuted and osteoporotic metaphysis [12,13], complications are not considerably decreased. To address this, physicians and scholars have explored and embraced the theory and clinical utilization of dual plates. Matthew and colleagues [14] discovered that the use of double-plate fixation in comminuted distal femur fractures significantly improved union rates and reduced the need for revision surgery. Nevertheless, the materials of implants commonly are non-biodegradable, such as titanium alloy, stainless steel, and cobalt-chromium alloy [15]. These implants could interact with the physiological environment over time and lead to adverse effects [16]. Additionally, after the healing process is complete, most patients require secondary surgery to remove or replace the implants, which adds further discomfort. Significant advancements have been made in developing biodegradable implants, including materials like Mg alloy, biopolymers, and bioceramics to address these challenges.

During the process of bone healing, biodegradable materials play a crucial role in offering initial mechanical support, gradually degrading as time passes. This degradation enables the bone to recover its original strength [17,18]. Especially bioresorbable composites have the advantage of promoting healing through the dissolved composition. Mechanical stability that resists the effect of compression, shear, and torsion is still critical to biodegradable materials [19], particularly in the application of fracture repair in weight-bearing joints. To date, none of the existing biodegradable materials have successfully combined high biocompatibility with optimal mechanical properties.

In order to improve the clinical management of fractures occurring in the distal femur and to provide guidance in the advancement of biodegradable materials, this study utilized finite element analysis to compare the mechanical effects of titanium-alloy implants and biodegradable implants in fixing physiological and osteoporotic distal femur fractures.

2. Materials and methods

2.1. Geometry and material properties

In order to establish a comprehensive 3D model of the femur, we conducted a scan on a left fourth-generation synthetic femur (3406#, Pacific Research Laboratories, Vashon, WA). This particular composite femur, widely utilized in biomechanical tests as an alternative to human bones, consisted of the cancellous bone made of polyurethane foam and the cortical bone comprised of e-glass fiber reinforced epoxy. Subsequently, we proceeded to create a fracture model following the AO/ASIF type 33-C2 specifications. This involved introducing a fracture gap measuring 1.5 cm, strategically positioned 6.5 cm to the joint line [20]. To integrate all the necessary components for the 3D representation, including implants and bones, we utilized the 3-matic software for assembly. We then used HyperMesh 11.0 (Altair Engineering, Inc., USA) to mesh these components, and nigraphics NX 8.5 (Siemens PLM) to reconstruct plates and screws. Finally, the fully assembled 3D models were imported into ANSYS software to generate the desired finite element models for analysis.

The fixation system included a prototype lateral plate that served as a reference for the LISS plate, as well as a medial plate modeled after the Proximal Humerus Internal Locking System (PHILOS) plate and the corresponding screws. All the implants were made of two kinds of material, titanium alloy (Ti-6AL-4V) and biodegradable material (Polylactide-based composites), which was developed for weight-bearing joints, and had an elastic modulus of 11.33 GPa and a Poisson ratio of 0.3 (Fig. 1). To explore different fixation

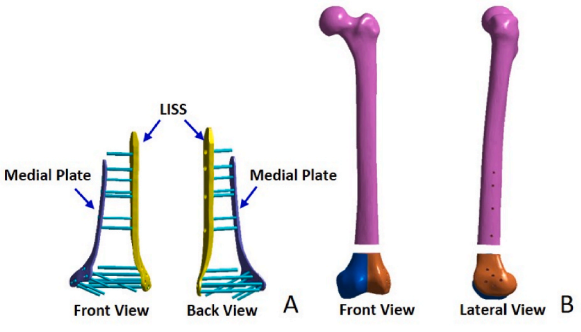

Fig. 1. Three-dimensional (A) plates, (B) AO/ASIF type 33-C2 fracture model.

scenarios, three models were constructed: LISS + TAP, LISS + BP, and DBPs, three-dimensional of fixation models of which were showed in Fig. 2(A-C). Both the plates and connecting screws shared the same material properties. Additionally, the femoral strengths were simulated under two conditions: physiological femur (PF) and osteoporotic femur (OF). In the OF model, Young's modulus of the cortical bone was reduced by 32%, while the cancellous bone's Young's modulus was decreased by 66% compared to the PF model [21]. The values of elastic modulus and Poisson's ratio are detailed in Table 1.

The fracture internal fixation model consisted of six components: cortical bone, trabecular bone, the lateral plate (LISS), the medial plate, screws of LISS, and screws of the medial plate. To create a mesh with a size of 1 mm, we utilized 187 tetrahedral solid elements. The determination of this grid size was based on mesh convergence testing. The meshes were segregated into five groups comprising grid sizes of 0.5 mm, 1 mm, 2 mm, 3 mm, and 5 mm. Ultimately, the difference in equivalent stress of the femoral and plate between the 1 mm and the 0.5 mm mesh was less than 5%, meeting the convergence criteria. Given considerations of computational efficiency and cost, a mesh size of 1 mm was selected. Table 2 presents the number of nodes for each component unit. It is crucial to emphasize that the number of elements and nodes in the three internal fixation models has no correlation with the material properties of the implants. Furthermore, frictional contact interactions between different parts of the model are assumed. The friction coefficient between simulated bones was set to 0.46, and the friction coefficient between bones and internal fixation was set to 0.3 [22,23].

2.2. Four-point bending

In order to assess the resistance of various models to forces exerted in a medio-lateral direction, we conducted two loadings with a downward tension of 350 N, simulating lateral loading of the physiological femur [24]. They were simultaneously applied at two distinct points: point A situated near the lesser trochanter, and point B located at distal femur, constrained by point C and point D at the quarter lengths of the femur with no displacement, representing medio-lateral four-point bending test (Fig. 3A). Similarly, two downward pulling forces of 350 N were vertically exerted on the model from the same two points on the anterior side of the coronal surface, and the fixation constrained from C'and D′, creating an antero-posterior four-point bending scenario (Fig. 3B). Moreover, we used three parameters, the peak VMS of lateral plate, the peak VMS and the maximum displacement of femur, to assess the performance of the different models under the applied loadings.

2.3. Axial loading

In order to evaluate the stability and strength of the fixation models, a load of 1500 N was applied to the middle of the femoral head to simulate typical walking loading forces, which were approximately 238% of 60 kg body weight [25]. T Fig. 4 presents the vector's orientation with an 8° inclination in the sagittal plane and a 13° inclination in the coronal plane in relation to the femoral shaft axis, and the distal femur was constrained with no further displacement. Furthermore, we measured five parameters to assess the effectiveness, including the axial stiffness, the peak VMS of the lateral plate, the bending angle in the coronal plane of the fracture, the peak VMS and the maximum displacement of femur (Fig. 5).

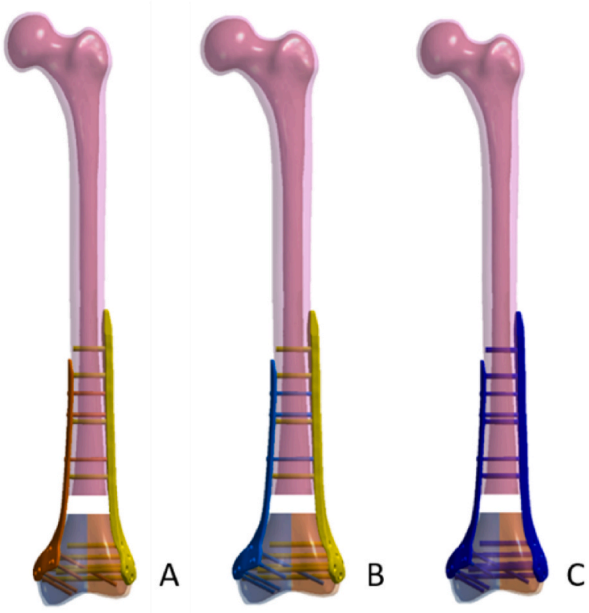

Fig. 2. Three-dimensional of fixation models (A) LISS + TAP, (B) LISS + BP, (C) DBPs.

Table 1
Material properties used in the study.

Material properties		E(GPa)	Poisson's ratio
physiological bone [21]	cortical bone	$E_1 = E_2 = 11.5$,E3 = 17	$V_{12} = 0.58$,V_{23}=V13 = 0.31
	cancellous bone	E = 2.13	V = 0.3
osteoporotic bone [21]	cortical bone	$E_1 = E_2 = 7.82$,E3 = 11.56	$V_{12} = 0.58$,V_{23}=V13 = 0.31
	cancellous bone	E = 0.724	V = 0.3
titanium alloy [22]	Ti-6AL-4V	105	0.35
biodegradable material	Polylactide-based composites	11.33	0.3

Table 2
Parameters of the FE models.

FE models	Elements	Nodes
Cortical bone	101299	170587
Trabecular bone	128394	190341
Lateral plate (LISS)	67608	103964
Medial plate	25924	44461
Screws of LISS	19748	34380
Screws of medial plate	7294	13623

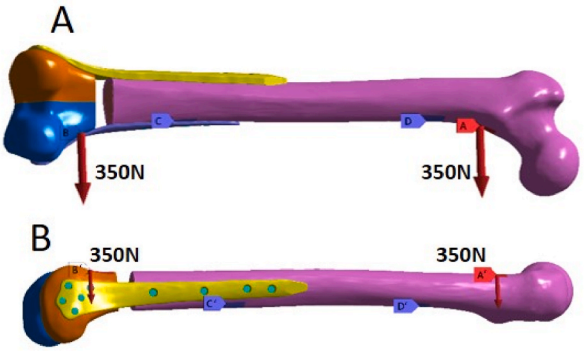

Fig. 3. Schematic diagram of (A) medio-lateral four-point bending and (B) antero-posterior four-point bending [20].

Fig. 4. The axial loading of 1500 N at the femoral head [20].

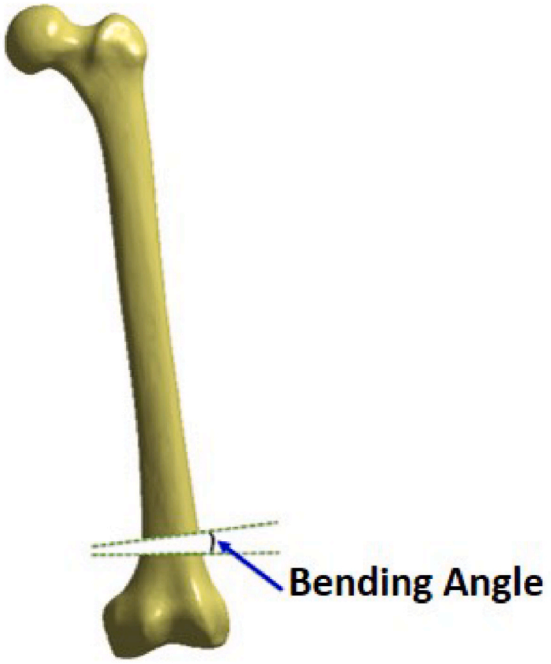

Fig. 5. Schematic diagram of the bending angle in the coronal plane of the fracture.

2.4. Torsional loading

In order to replicate the physiological transition from sitting to standing, the model underwent torsional loading of 150 Nm at the centre of the femoral head, while preventing displacement at the end of the femur. It's worth noting that the simulation disregarded the influences of several muscle groups (Fig. 6). In addition, we used six parameters to evaluate the patterns' deformation, including the torsional stiffness, the peak VMS of lateral plate, the maximum torsional angle of the femoral head, the torsional angle of fracture, the peak VMS and the maximum displacement of femur (Fig. 7).

2.5. Sideways falling

To study the effect of force transfer on distal femoral fractures, we performed a side-drop experiment in which the femoral neck was rotated medially by 15° and the femoral shaft was aligned along the horizontal plane by 10° (Fig. 8). Model simulations were performed using methods described in existing literature [26,27], the greater trochanter was held vertically to reestablish the contact surface during impact and the stationary model was allowed to move in the horizontal plane without rotating around the shaft axis. A force of 3750 N was exerted on the center of the femoral head's inferior surface to simulate a fall equivalent to a body weight of 60 Kg. We borrowed three parameters to present the experimental results: the peak VMS of the lateral plate, the peak VMS and the maximum displacement of femur.

2.6. Risk of fracture calculation

Fracture has been determined by strain [28]. To assess the risk of fracture, we defined a scalar quantity called Risk of Fracture (RF).

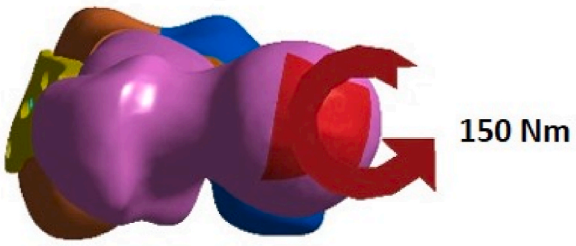

Fig. 6. The 150 Nm torsional loading at the middle of the femoral head [20].

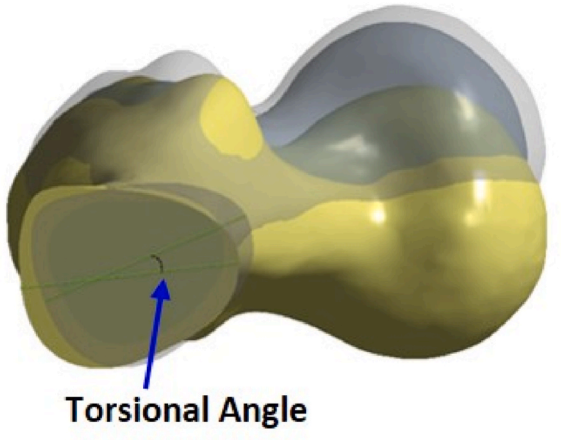

Fig. 7. The torsional angle diagram of the fracture of the bone models [20].

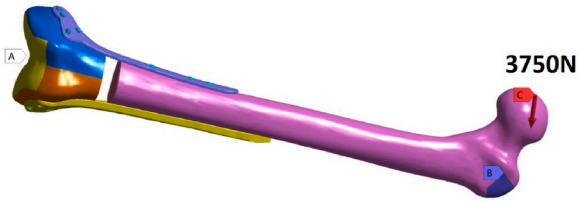

Fig. 8. Schematic diagram of finite element model of sideways falling with the 3750 N loading vector.

RF is computed as the ratio between the maximum principal strain within the femur shaft (compressive or tensile) and the corresponding ultimate strain [29,30].

$RF = \varepsilon_{max}/\varepsilon_{lim.}$

ε_{max} stands for the maximum principal strain of the femur; ε_{lim} is the ultimate strain, representing different values for compressive and tensile conditions. As previous studies [30,31], the ultimate tensile strain ($\varepsilon_{lim\text{-}Tensile} = 0.0073$) was taken as 70% of the ultimate compressive strain ($\varepsilon_{lim\text{-}Compressive} = 0.0104$), and fundamentally, $RF < 1$ is the safeguard to prevent fracture. Moreover, Microsoft Office Excel 2013 was utilized to create all the statistical diagrams.

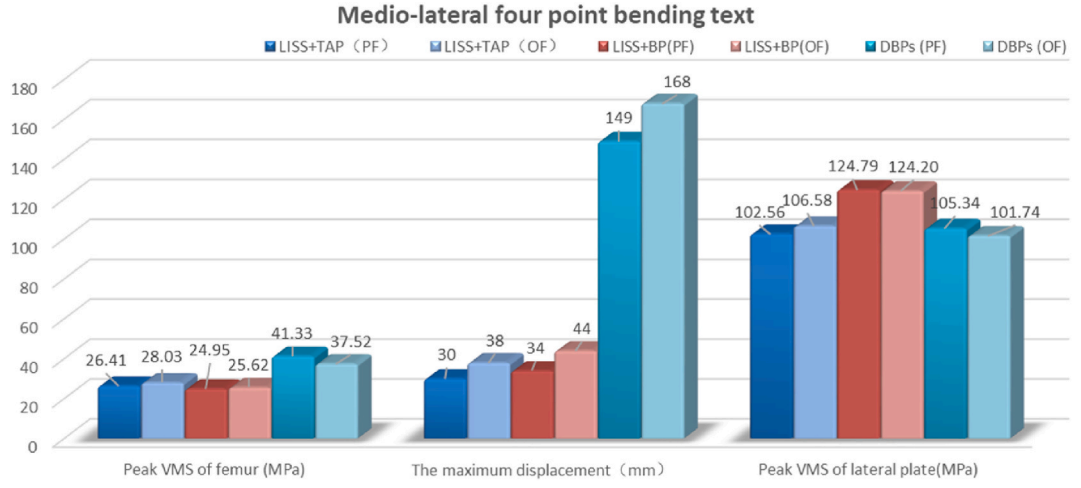

Fig. 9. The peak VMS of femur (MPa), the maximum displacement (mm), and the peak VMS of lateral plate (MPa) were demonstrated in the medio-lateral four-point bending test, with the different colors representing different scenarios. The maximum displacement values have been multiplied by 100 to make them comparable.

3. Results

3.1. Medio-lateral four-point bending test

Except for DBPs, the values of all three parameters were virtually greater in the osteoporotic femur than in the physiological femur. The peak VMS of femur and the maximum displacement of DBPs were all the highest among all three types of fixation models, regardless of whether it was a physiological or osteoporotic femur. Specifically, the values of the peak VMS of femur in the DBPs (PF) and DBPs (OF) groups were approximately 1.5 times greater measurements compared to the remaining groups. Moreover, the peak VMS of lateral plate values of the LISS + BP group was slightly higher than the LISS + TAP and DBPs groups. Notably, the maximum displacement of DBPs (PF) was 5 times greater than that of LISS + TAP (PF), and the value of DBPs (OF) was more than 4 times higher than that in the LISS + TAP (PF) (Fig. 9). Furthermore, it is worth noting that the maximum displacement occurred in the femoral condyle and head region, and the peak VMS of both lateral plates and femurs values were concentrated in the defect area.

3.2. Antero-posterior four-point bending test

Among all the configurations, DBPs patterns provided the highest values for the peak VMS of femur and the maximum displacement while exhibiting the lowest peak VMS of lateral plate. Specifically, for the normal bone condition, the peak VMS of femur in DBPs was 2.33 times and 2.88 times higher than LISS + TAP and LISS + BP constructs and 2.1 times and 2.22 times for the osteoporotic bone. Moreover, under both normal and osteoporotic conditions, the maximum displacement of DBPs was respectively over 500% and almost 300% greater than LISS + TAP and LISS + BP. However, the peak VMS of lateral plate in DBPs (PF) and DBPs (OF) were 37% and 40% lower than that of LISS + BP (PF) and LISS + BP (OF), respectively, which were almost equivalent to the values in the LISS + TAP (PF) and LISS + TAP (OF) groups (Fig. 10). Similar to the medio-lateral four-point bending test, the maximum displacement concentrated in the region of femoral condyle and head, and the peak VMS values were occurred in the defect area, affecting both the lateral plate and the femur.

3.3. The axial loading test

Fig. 4A illustrated the comparison of axial stiffness among different constructs. The LISS + TAP construct demonstrated significantly superior stiffness, with LISS + TAP (OF) values being 1.42 times and 1.86 times greater than LISS + BP (OF) and DBPs (OF) respectively (Fig. 11A). Additionally, the osteoporotic femur exhibited reduced rigidity compared to the physiological femur. In the osteoporotic bone, the peak VMS of DBPs construct was 183% and 17% greater than LISS + TAP and LISS + BP respectively, with maximum stresses consistently observed around the fracture sites (Fig. 11B). And the peak VMS of lateral plate in DBPs (OF) construct was 2% and 16% lower than LISS + TAP (OF) and LISS + BP (OF), respectively (Fig. 11C). Moreover, parameters of bending angle and the maximum displacement increased with the number of biodegradable plates and presence of osteoporosis, indicating micromotion in all fixation models (Fig. 11D). Specifically, for the maximum displacement, the values of DBPs (PF) was respectively 36% and 114% higher than LISS + BP (PF) and LISS + TAP (PF); DBPs (OF) was respectively 31% and 86% greater than LISS + BP (OF) and LISS + TAP (OF). What's more, for the bending angle in the physiological femur, DBPs had values of 25% and 105%, respectively, higher than LISS + BP and LISS + TAP. In contrast, in the osteoporotic femur, the values were 13% and 63% higher (Fig. 11E). Moreover, the VMS and

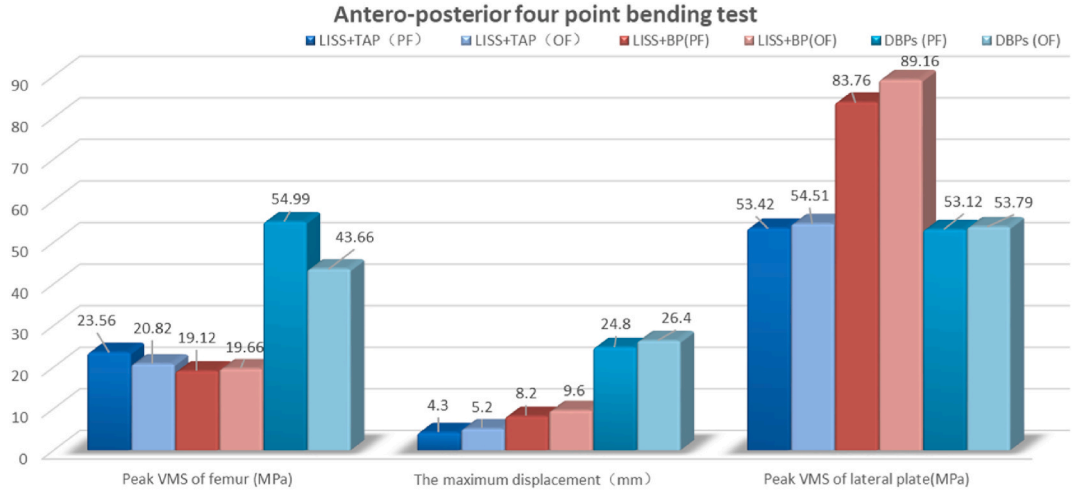

Fig. 10. The peak VMS of femur (MPa), the maximum displacement (mm), and the peak VMS of lateral plate (MPa) of the three groups of patterns under antero-posterior four-point bending. Different colors stand for other models, and the maximum displacement values are all enlarged by 10 times.

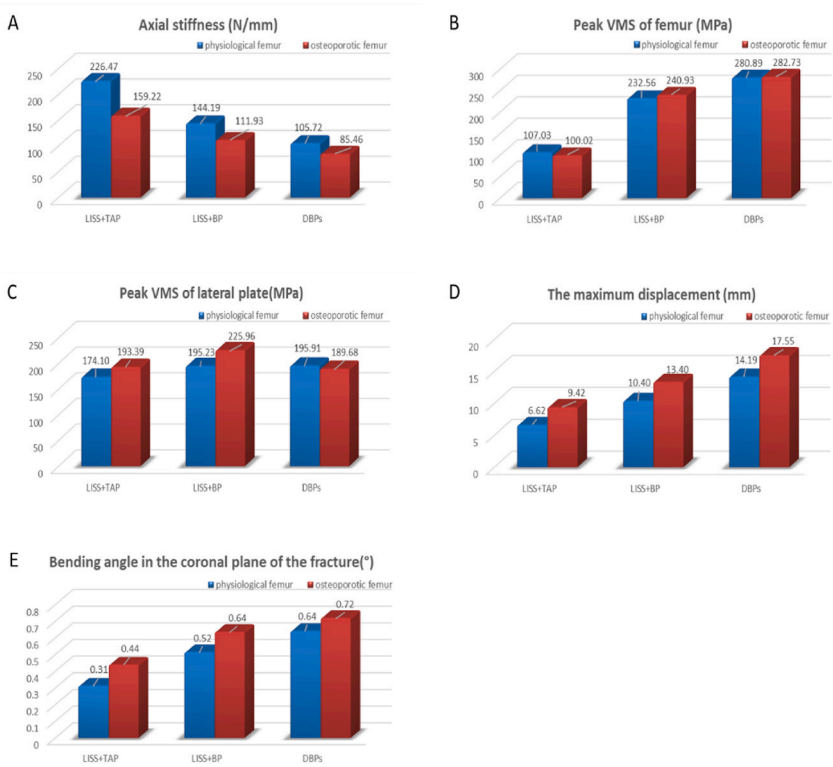

Fig. 11. The results of axial loading of 1500 N. (A) Axial stiffness was measured as the ratio of the applied load to the maximum displacement; Comparison of the construct axial strength and micromotion of all models with (B) the peak VMS of femur, (C) the peak VMS of Lateral plate, (D) the maximum displacement, and (E) the bending angle in the coronal plane of the fracture.

displacement of the femur exhibited a gradual decrease from the femoral head, while the femoral condyle experienced minimal strain and stress. Additionally, the peak VMS of plates was primarily around the defective area of the middle and lower femur.

3.4. The torsional loading test

Similar to axial loading, the application of biodegradable plates significantly impacted the anti-torsional effect of fixation models. The rotational stiffness of DBPs (PF) was found to be 66% higher than that of LISS + TAP (PF) and 69% higher than that of LISS + BP (PF). In comparison, the rotational stiffness of DBPs (OF) was 2% higher than LISS + TAP (OF) and 52% higher than LISS + BP (OF) (Fig. 12A). In terms of the peak VMS of femur, the values of DBPs (PF) and DBPs (OF) were respectively 17% and 8% lower respectively compared to LISS + TAP (PF) and LISS + TAP (OF), and 23% and 15% lower compared to LISS + BP (PF) and LISS + BP (OF) (Fig. 12B). Furthermore, when considering the peak VMS of lateral plates, DBPs (PF) and DBPs (OF) were found to be 11% and 6% higher respectively than LISS + TAP (PF) and LISS + TAP (PF), but 16% and 14% lower respectively than LISS + BP (PF) and LISS + BP (OF) (Fig. 12C).

Osteoporosis had a significant impact on the micromotion of all fixation constructs under torsional loading. The lowest increase in displacement was found in LISS + BP (from 16.92 mm to 21.79 mm, 129%). The LISS + TAP (from 14.10 mm to 18.76 mm, 133%) and DBPs (9.74 mm–13.80 mm, 142%) (Fig. 12D). To analyze the variations in torsion at different sites, we examined the maximum torsional angle of femoral head (Fig. 12E) fracture (Fig. 12F). Notably, DBPs provided the highest torsional angle of the femoral head (ranging from 4.93° to 8.59°, 174%), contrasting with LISS + TAP (from 8.18° to 8.75°, 107%) and LISS + BP (from 8.35° to 13.07°, 157%). Additionally, DBPs demonstrated the highest torsional angle of the fracture, ranging from 0.04° to 0.18° (467%), in comparison to LISS + TAP (from 0.06° to 0.07°, 117%) and LISS + BP (from 0.06° to 0.28°, 441%).

The femoral head was the primary location for the peak VMS and displacement in the femur, distributed in a ladder-like fashion along the torsion direction throughout the femur. In contrast, the plate experienced peak VMS concentrated in the site of the femoral defect, and the lateral titanium alloy plate exhibited the smallest range of stress distribution.

3.5. Sideways falling test

Under this loading condition, the parameters of fixation models for osteoporotic femur were consistently higher than those for normal bone. Regarding the peak VMS of femur (Fig. 13A) and the maximum displacement (Fig. 13B), the results of DBPs (PF) were

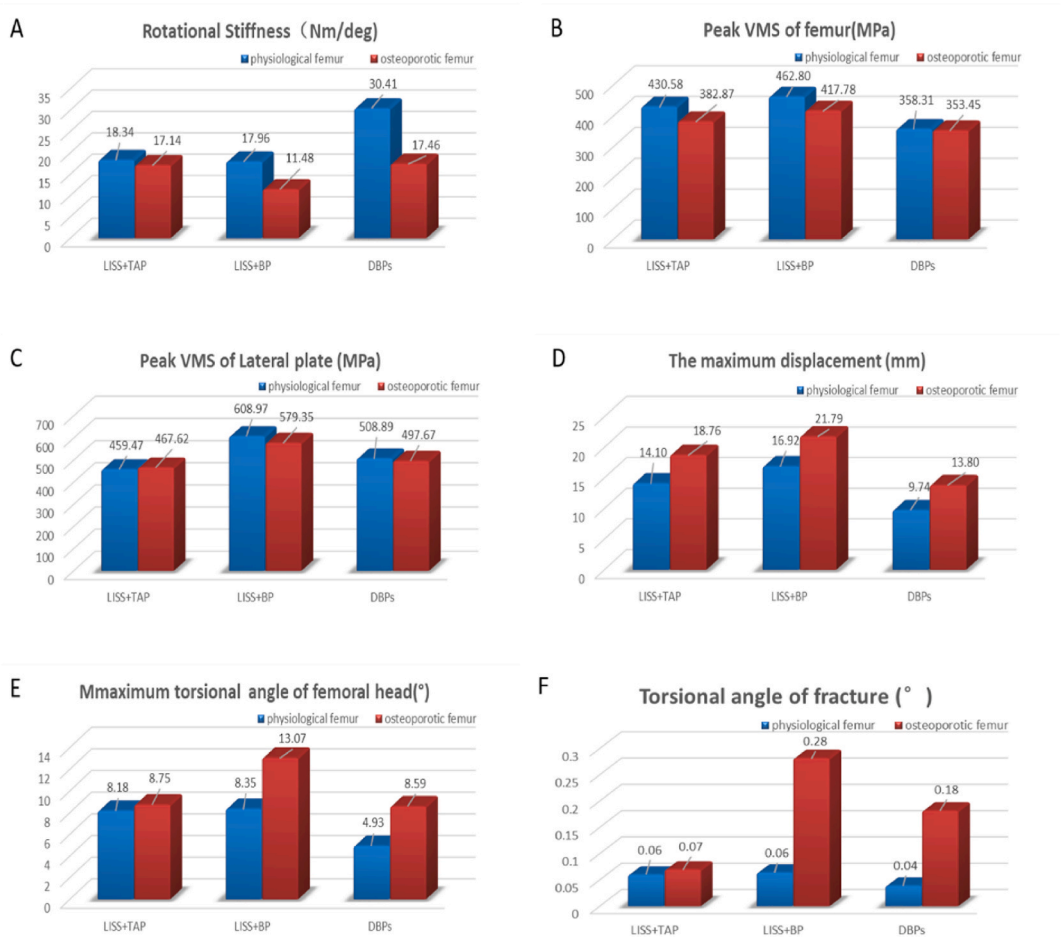

Fig. 12. The results of the torsional loading of 150 Nm. (A) The torsional stiffness was measured as the ratio of the applied load to the maximum torsional angle of femoral head; (B) the peak VMS of femur and (C) the peak VMS of Lateral plate showed fixation model bearing capacity; (D) the maximum displacement, (E) the maximum torsional angle of femoral head and (F) the torsional angle of fracture represented the micromotions.

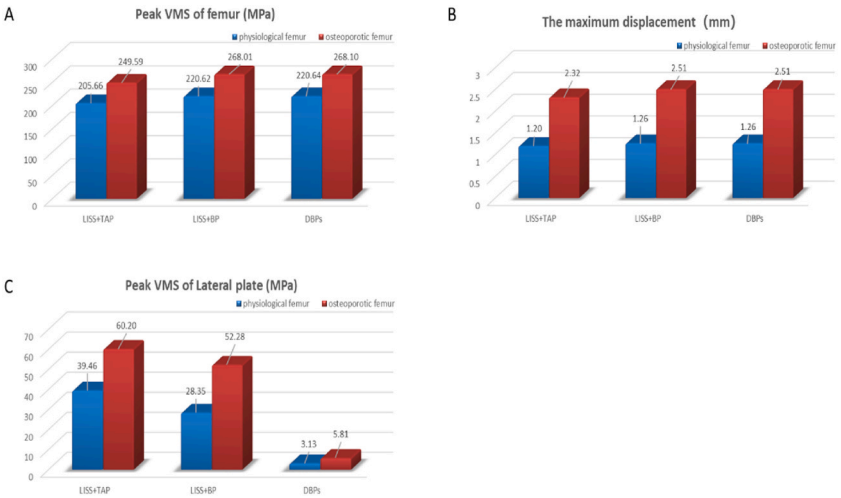

Fig. 13. The outcomes of the sideways falling of 3750 N. (A) The peak VMS of femur, (B) the maximum displacement and (C) the peak VMS of lateral plate together illustrate the stability of the different fixation models.

roughly equal to LISS + TAP (PF) and LISS + BP (PF), and those of DBPs (OF) were essentially the same as the other two models for osteoporotic bone. However, there were notable variations in the values of the peak VMS for lateral plates among different scenarios (Fig. 13C). Specifically, that of DBPs (PF) construct was approximately 92% and 89% lower compared to the LISS + TAP (PF) and LISS + BP (PF) constructs, respectively. Additionally, the peak VMS for the LISS + TAP (OF) construct was 90% and 89% lower compared to the LISS + TAP (OF) and LISS + BP (OF) constructs, respectively. The peak VMS and displacement for all models consistently occurred around the greater trochanter.

3.6. Risk of fracture

Fig. 14 presented the RF values of different models across all five tests and compared the maximum RF values between physiological and osteoporotic material models. Overall, osteoporosis significantly increased the risk of fractures for all the scenarios, with most fixation models tending to fail under axial and torsional loading. In particular, the RF values of LISS + TAP were consistently lower than those of LISS + BP and DBPs, and an enormous difference was observed in the axial loading test, where the RF values of LISS + BP (PF) and DBPs (PF) were 152% and 194% respectively larger than LISS + TAP (PF). Contrarily, during torsional stress, the RF value of DBPs (PF) was 19.6% and 26%, respectively, lower than that of LISS + TAP (PF) and LISS + BP (PF). Notably, the data from the three fixation models in the sideways failing experiment were the same. However, the RF values of the osteoporosis models were approximately 70% higher than those of physiological scenarios. Similarly, RF value of DBPs (PF) was found to be 19.6% and 26% lower than that observed in LISS + TAP (PF) and LISS + BP (PF) in torsional loading test. Furthermore, there were no significant differences in the data among the three fixation models in the sideways failing experiment, and of course, the RF values of the osteoporosis models were approximately 70% greater than physiological models.

4. Discussion

In this study, several fixation conditions and material properties configurations were examined to assess their relative outcomes. The objective was to appraise the structural stability of dual-plate fixations (titanium alloy and biodegradable material) for distal femur fractures, considering both physiological and osteoporotic cases, with three main categories of indexes: structural stiffness, fracture micromotion, and implant stress. This will give a theoretical foundation for treating distal femur fractures with osteoporosis and guide the development of bioabsorbable materials.

4.1. Mechanical analysis of fracture fixations

Regarding structural stability, the osteoporotic scenarios exhibited decreased rigidity and increased micromotion. This can explain the role of fatigue damage in internal fixation failure, nonunion, and peri-implant fracture. Elkins et al. [32] carried out an examination using finite element analysis to imitate supracondylar femoral fractures that were treated with fixation using a locking plate, and they deduced that longitudinal movement encouraged the development of callus while shear motion hindered callus formation. Generally, the longitudinal strain of the fracture gap should be less than 10% [33] and the displacement between fracture fragments should be 0.2–1.0 mm [34,35], which are conditions conducive to callus formation. According to these, it can be concluded that double plates serve as an effective initial fixation method for the treatment of osteoporotic fractures of the distal femur, resulting from bending angle, torsional angle, and stiffness values. However, too-elastic fixation lacks stability, while overly rigid fixation can suppress callus formation [36]. Consequently, a thorough understanding of interfragmentary movements during rehabilitation, especially under partial weight-bearing, can help determine the proper construct that provides optimal healing potential [9]. From another perspective, developing new fixations with appropriate mechanical strength, like biodegradable plates, is necessary to address these challenges.

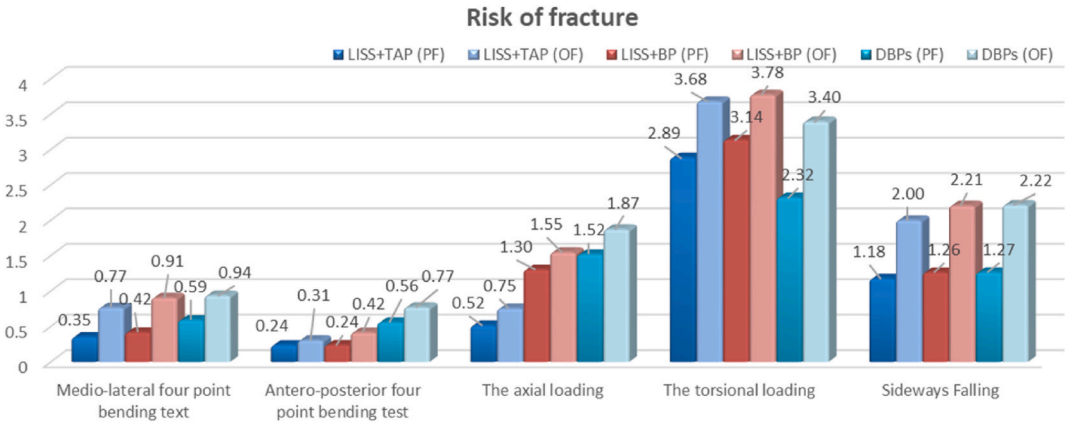

Fig. 14. Risk of fracture (RF) of all the configurations with both physiological and osteoporotic femur.

Based on the sideways falling test, we observed that both osteoporotic and physiological bone models exhibited maximum displacement and peak VMS of femur concentrated at the greater trochanter, with no discernible force transmission observed at the distal femur. It is noteworthy that in the torsion test, the overall stiffness of the osteoporosis model was lower, making it more prone to deformation than the physiological bone model. As a result, the peak VMS observed in the lateral plate and femur were smaller in the osteoporotic femur compared to the physiological femur. Rather than indicating local variations in axial compression or four-point bending, we hypothesize that the torsion test provides a more robust prediction of the overall characteristics of the fixation.

4.2. Mechanical analysis of biodegradable implants

The ideal solution is to have biodegradable the implants offer sufficient mechanical support during the entire healing process and degrade promptly following the completion of healing [19]. Therefore, the initial strength of biodegradable plates plays a crucial role. Based on the results from the other four mechanical experiments, excluding the torsional test, it can be inferred that in terms of initial strength, the peak VMS of lateral plates of DBPs did not significantly increase compared to LISS + TAP, while in contrast, the axial and rotational stiffness of the fixed model decreased along with increased the peak VMS of femur and micromotion of the scenario. However, in torsional experiments, the DBPs fixation demonstrated even higher structural stiffness and less micro-movement than the LISS + TAP. In contrast, the mechanical effect of LISS + BP fell between the two aforementioned models. We hypothesize that, unlike metal implants, which tend to bear the majority of the mechanical stress and preclude shielding the surrounding bone from normal pressure [37–39], biodegradable ones could contribute to load-stimulated bone remodeling, which would mitigate the effect of "stress-shielding".

Some studies on absorbable materials have primarily focused on examining the materials' properties, degradation rules, biological activity, engineering preparation, etc., while neglecting to consider the biomechanical strength requirements in the human body. A comprehensive comprehension concerning the interconnections among the structure, processing circumstances, and ultimate characteristics of Poly (L-lactide-*co*-D, L-lactide) PDLA/45S5 Bioglass was revealed by X. L. Andreu et al. [40]. They demonstrated the biomechanical strength of the biomaterial, like Young's modulus and stresses, through mechanical analyses using different bioglass content. While these findings are valuable, it is essential to simulate absorbable materials' mechanical strength within a fixed model. This approach would be more beneficial for further material modification and design endeavors.

People who have osteoporosis typically experience reduced bone strength, and the metal implant model demonstrated slightly higher overall rigidity compared to the internal bioabsorbable-implants fixation model, making it less prone to deformation. To improve the initial stability of the biodegradable plate (My-alloy), Girish Chandra et al. [41,42] employed an embossed structure with a semicircular filleted design at the longitudinal center.Our study highlights the importance of fatigue resistance property in addition to initial strength. Therefore, we recommend combining metal and biodegradable internal fixation, such as LISS + BP, as an effective strategy to synergize the advantages offered by both materials.

4.3. Risk of fracture

We conducted simulations for five mechanical scenarios, including medio-lateral force, antero-posterior stress, total weight-bearing walking, movement from sitting to standing up, and sideways falling, to assess the risk of internal fixation failure based on principal strain, which could be valuable in guiding postoperative rehabilitation programs. Presently, there remains an absence of established guidelines and consensus regarding the management of postoperative cases related to complicated distal femoral fractures, particularly concerning the implementation of safe weight-bearing protocols aimed at mitigating both mortality and morbidity rates [9,11]. For patients undergoing conventional dual plate fixation for type C3 fractures, we do not recommend full weight-bearing, sitting up, and walking until the defect has adequately healed. During the sideways falling test, the risk of hip fracture was illustrated instead of fixation failure in the distal femur, as the stress was primarily concentrated on the greater trochanter.

On the other hand, since soft tissues can attenuate the forces exerted on the femur during a fall, the magnitude of the external force exerted on the femur may also depend on the direction of impact [27,43], which was neglected to facilitate the investigating of force transmission across the distal femur. In conclusion, we have demonstrated that unless the distal femur is directly impacted or damaged, the force will not transfer through the femur to damage the internal fixation system. Moreover, through experimental analysis, we have strong indications that the absorbable plate with Young's modulus of 11.33 GPa can sufficiently meet the weight-bearing joints' early basic strength requirements.

4.4. Limitations

The study presented in this paper had a few limitations. For instance, the patterns used in the study were constructed using a femur model made from composite material, which may not fully replicate the complexities of the standard human skeletal structure and its response to actual fractures; in addition, we did not take degradation and healing process into consideration, which could impact the stability of fixation models; furthermore, the neglect of soft tissues and ligaments surrounding the fracture, to a certain extent, deviated from the realistic physiological environment of the fracture.

5. Conclusion

Overall, dual plates exhibited outstanding mechanical efficacy when utilized for the restoration of osteoporotic femurs, rendering

them a feasible therapeutic alternative for comminuted fractures of the distal femur among elderly individuals. In particular, double biodegradable plates with 11.33 GPa allowed for early mobilization of weight-bearing joints, although complete weight-bearing physiological activities may not be recommended. The LISS + TAP technique provided practical strength requirements for the repair, but it is essential to consider the potential biological irritation and stress-shielding effects associated with this approach. From a biomechanical and material perspective, combining biodegradable and metal internal fixation is a valid approach for clinically managing weight-bearing joint fractures.

These biomechanical results have significant implications for improving current clinical treatment strategies and advancing the field of bioabsorbable materials.

Funding

This study was funded by Research on remote orthopedic surgical robot for modern battlefield treatment (16CXZ043)

CRediT authorship contribution statement

Mengmeng Hu: Methodology. **Meng Li:** Writing – original draft. **Rui Ma:** Investigation. **Xiaoya Li:** Formal analysis. **Xiaomeng Ren:** Software. **Longbo Du:** Software. **Chuyang Zeng:** Methodology. **Jiantao Li:** Supervision. **Wei Zhang:** Formal analysis, Validation, Writing – review & editing.

Declaration of competing interest

The authors declare the following financial interests/personal relationships which may be considered as potential competing interests:Wei Zhang reports financial support was provided by Fourth Medical Center of PLA General Hospital. Wei Zhang reports a relationship with Fourth Medical Center of PLA General Hospital that includes: employment. If there are other authors, they declare that they have no known competing financial interests or personal relationships that could have appeared to influence the work reported in this paper.

References

[1] O. Martinet, J. Cordey, Y. Harder, A. Maier, M. Bühler, G.E. Barraud, The epidemiology of fractures of the distal femur, Injury 31 (Suppl 3) (2000) C62–C63.
[2] D. Wahnert, K. Hoffmeier, R. Frober, G.O. Hofmann, T. Muckley, Distal femur fractures of the elderly–different treatment options in a biomechanical comparison, Injury 42 (2011) 655–659.
[3] P.N. Streubel, W.M. Ricci, A. Wong, M.J. Gardner, Mortality after distal femur fractures in elderly patients, Clin. Orthop. Relat. Res. 469 (2011) 1188–1196.
[4] J.L. Marsh, T.F. Slongo, J. Agel, J.S. Broderick, W. Creevey, T.A. DeCoster, L. Prokuski, M.S. Sirkin, B. Ziran, B. Henley, L. Audigé, Fracture and dislocation classification compendium - 2007: orthopaedic Trauma Association classification, database and outcomes committee, J. Orthop. Trauma 21 (2007) S1–S133.
[5] R. Brumback, S. Uwagie-Ero, R. Lakatos, A. Poka, G. Bathon, A.J.T. Job Burgess, J.S.A. Volume, Intramedullary nailing of femoral shaft fractures, Part II: Fract. Heal. Static interlock. Fix. 70 (1988) 1453–1462.
[6] M. Gardner, S. Boraiah, D. Helfet, D.J. Joot Lorich, Indirect medial reduction and strut support of proximal humerus fractures, using an endosteal implant 22 (2008) 195–200.
[7] R. Meneghini, B. Keyes, K. Reddy, Modern retrograde intramedullary nails versus periarticular locked plates for supracondylar femur fractures, after total knee arthroplasty 29 (2014) 1478–1481.
[8] C.M. Court-Brown, M.M. McQueen, Global Forum: fractures in the elderly, J Bone Joint Surg Am 98 (2016) e36.
[9] D. Todorov, I. Zderic, R.G. Richards, M. Lenz, M. Knobe, D. Enchev, A. Baltov, B. Gueorguiev, K. Stoffel, Is augmented LISS plating biomechanically advantageous over conventional LISS plating in unstable osteoporotic distal femoral fractures? J. Orthop. Res. 36 (2018) 2604–2611.
[10] S.H. Chen, M.C. Chiang, C.H. Hung, S.C. Lin, H.W. Chang, Finite element comparison of retrograde intramedullary nailing and locking plate fixation with/without an intramedullary allograft for distal femur fracture following total knee arthroplasty, Knee 21 (2014) 224–231.
[11] J.R. Smith, R. Halliday, A.L. Aquilina, R.J. Morrison, G.C. Yip, J. McArthur, P. Hull, A. Gray, M.B. Kelly, S. Collaborative - Orthopaedic Trauma, Distal femoral fractures: the need to review the standard of care, Injury 46 (2015) 1084–1088.
[12] E. Fulkerson, K. Koval, C. Preston, K. Iesaka, F. Kummer, K.J.J.o.o.t. Egol, Fixation of periprosthetic femoral shaft fractures associated with cemented femoral stems: a biomechanical comparison of locked plating and conventional cable plates 20 (2006) 89–93.
[13] M. Zlowodzki, S. Williamson, L.D. Zardiackas, P.J. Kregor, Biomechanical evaluation of the less invasive stabilization system and the 95-degree angled blade plate for the internal fixation of distal femur Fractures in human cadaveric bones with high bone mineral density, J. Trauma 60 (2006) 836–840.
[14] M. Bologna, M. Claudio, K. Shields, C. Katz, T. Salopek, E.J.J.o.o. Westrick, Dual plate fixation results in improved union rates in comminuted distal femur fractures compared to single plate fixation 18 (2020) 76–79.
[15] R. Radha, D. Sreekanth, Insight of magnesium alloys and composites for orthopedic implant applications – a review, J. Magnesium Alloys 5 (2017) 286–312.
[16] H. Nieto, C. Baroan, Limits of internal fixation in long-bone fracture, Orthop Traumatol Surg Res 103 (2017) S61–S66.
[17] T.J. Lehtonen, J.U. Tuominen, E. Hiekkanen, Dissolution behavior of high strength bioresorbable glass fibers manufactured by continuous fiber drawing, J. Mech. Behav. Biomed. Mater. 20 (2013) 376–386.
[18] X.Y. Cao, N. Tian, X. Dong, C.K. Cheng, Polylactide composite pins reinforced with bioresorbable continuous glass fibers demonstrating bone-like apatite formation and spiral delamination degradation, Polymers (2019) 11.
[19] G. Chandra, A. Pandey, S. Pandey, Design of a biodegradable plate for femoral shaft fracture fixation, Med. Eng. Phys. 81 (2020) 86–96.
[20] M. Li, Y. Jiang, J. Wang, G. Xu, D. Wang, J. Li, W. Zhang, Finite Element Analysis of Different Medial Fixation Strategies in Double-Plate Osteosynthesis for AO Type 33-C2 Fractures, Injury, 2022.
[21] E. Bori, F. Armaroli, B. Innocenti, Biomechanical analysis of femoral stems in hinged total knee arthroplasty in physiological and osteoporotic bone, Comput. Methods Progr. Biomed. 213 (2022) 106499.
[22] W. Zhang, J. Li, H. Zhang, M. Wang, L. Li, J. Zhou, H. Guo, Y. Li, P. Tang, Biomechanical assessment of single LISS versus double-plate osteosynthesis in the AO type 33-C2 fractures: a finite element analysis, Injury 49 (2018) 2142–2146.
[23] J. Goffin, P. Pankaj, A.J.J.o.o.r.o.p.o.t.O.R.S. Simpson, The importance of lag screw position for the stabilization of trochanteric fractures with a sliding hip screw, a subject-specific finite element study 31 (2013) 596–600.
[24] E. Steinhauser, P. Diehl, M. Hadaller, J. Schauwecker, R. Busch, R. Gradinger, W. Mittelmeier, Biomechanical investigation of the effect of high hydrostatic pressure treatment on the mechanical properties of human bone, J. Biomed. Mater. Res. B Appl. Biomater. 76B (2006) 130–135.

[25] J. Lu, S.C. Guo, Q.Y. Wang, J.G. Sheng, S.C. Tao, J-bone graft with double locking plate: a symphony of mechanics and biology for atrophic distal femoral non-union with bone defect, J. Orthop. Surg. Res. 15 (2020) 144.
[26] M. Soenen, M. Baracchi, R. De Corte, L. Labey, B. Innocenti, Stemmed TKA in a femur with a total hip arthroplasty: is there a safe distance between the stem tips? J. Arthroplasty 28 (2013) 1437–1445.
[27] C. Ford, T. Keaveny, W.J.J.o.b. Hayes, m.r.t.o.j.o.t.A.S.f. Bone, M. Research, The effect of impact direction on the structural capacity of the proximal femur, during falls 11 (1996) 377–383.
[28] R.K. Nalla, J.H. Kinney, R.O. Ritchie, Mechanistic fracture criteria for the failure of human cortical bone, Nat. Mater. 2 (2003) 164–168.
[29] E. Schileo, E. Dall'ara, F. Taddei, A. Malandrino, T. Schotkamp, M. Baleani, M. Viceconti, An accurate estimation of bone density improves the accuracy of subject-specific finite element models, J. Biomech. 41 (2008) 2483–2491.
[30] H.H. Bayraktar, E.F. Morgan, G.L. Niebur, G.E. Morris, E.K. Wong, T.M. Keaveny, Comparison of the elastic and yield properties of human femoral trabecular and cortical bone tissue, J. Biomech. 37 (2004) 27–35.
[31] C.M. Ford, T.M. Keaveny, W.C. Hayes, The effect of impact direction on the structural capacity of the proximal femur during falls, J. Bone Miner. Res. 11 (1996) 377–383.
[32] J. Elkins, J.L. Marsh, T. Lujan, R. Peindl, J. Kellam, D.D. Anderson, W. Lack, Motion predicts clinical callus formation: construct-specific finite element analysis of supracondylar femoral fractures, J Bone Joint Surg Am 98 (2016) 276–284.
[33] S.J.T. Job Perren, J.S.B. Volume, Evolution of the internal fixation of long bone fractures, The scientific basis of biological internal fixation: choosing a new balance between stability and biology 84 (2002) 1093–1110.
[34] M. Bottlang, J. Doornink, T.J. Lujan, D.C. Fitzpatrick, J.L. Marsh, P. Augat, B. von Rechenberg, M. Lesser, S.M. Madey, Effects of construct stiffness on healing of fractures stabilized with locking plates, J Bone Joint Surg Am 92 (Suppl 2) (2010) 12–22.
[35] L. Claes, C. Heigele, C. Neidlinger-Wilke, D. Kaspar, W. Seidl, K. Margevicius, P.J.C.o. Augat, r. research, Effects of Mechanical Factors on the Fracture Healing Process, 1998, pp. S132–S147.
[36] J.J.J.o.o.t. Krieg, Locked plating of distal femur fractures leads to inconsistent and asymmetric callus formation 25 (2011) e21. ; author reply e21-22.
[37] F. Lin, T. Chen, C. Lin, C.J.A.o. Lee, The merit of sintered PDLLA/TCP composites in management of bone fracture internal fixation 23 (1999) 186–194.
[38] J. Hayes, R.J.E.r.o.m.d. Richards, The use of titanium and stainless steel in fracture fixation 7 (2010) 843–853.
[39] A. Barbas, A. Bonnet, P. Lipinski, R. Pesci, G.J.J.o.t.m.b.o.b.m. Dubois, Development and mechanical characterization of porous titanium bone substitutes 9 (2012) 34–44.
[40] X. Lacambra-Andreu, N. Dergham, M. Magallanes-Perdomo, S. Meille, J. Chevalier, J.M. Chenal, A. Maazouz, K. Lamnawar, Model composites based on poly (lactic acid) and bioactive glass fillers for bone regeneration, Polymers 13 (2021).
[41] G. Chandra, A. Pandey, Biomechanical evaluation on a novel design of biodegradable embossed locking compression plate for orthopaedic applications using finite element analysis, Biomech. Model. Mechanobiol. 21 (2022) 1371–1392.
[42] G. Chandra, A. Pandey, N. Tipan, Longitudinally centered embossed structure in the locking compression plate for biodegradable bone implant plate: a finite element analysis, Comput. Methods Biomech. Biomed. Eng. 25 (2022) 603–618.
[43] S. Robinovitch, T. McMahon, W.J.J.o.o.r.o.p.o.t.O.R.S. Hayes, Force attenuation in trochanteric soft tissues during impact from a fall 13 (1995) 956–962.